

GT2004-53579

AERODYNAMIC AND MECHANICAL VIBRATION ANALYSIS OF A COMPRESSOR BLISK AT SURGE

Harald Schöenborn
MTU Aero Engines GmbH
Dachauer Strasse 665
D-80995 Muenchen, Germany
+49 89 1489 8326, +49 89 1489 99414
Harald.Schoenenborn@muc.mtu.de

Thomas Breuer
MTU Aero Engines GmbH
Dachauer Strasse 665
D-80995 Muenchen, Germany
+49 89 1489 2637, +49 89 1489 97643
Thomas.Breuer@muc.mtu.de

ABSTRACT

Typically surge events in compressors are investigated only from the aerodynamic point of view (aerodynamic instability or lack of surge margin). For this assessment various methods exist during the design phase. For the analysis of the structural impact of surge in this phase the situation is more challenging, because an analytical prediction of the blade loading during surge is difficult to obtain. In this paper a combined analysis of aerodynamic and structural aspects of surge in compressor rotor blades of advanced axial flow compressors with state-of-the-art numerical procedures is presented and compared to extensive strain-gauge measurements.

The unsteady aerodynamic excitation of a compressor rotor blade during surge is determined with a numerical procedure which allows calculating the unsteady flow field in a compression system. Blade rows of the compressor are simulated by appropriate loss/deviation characteristics covering both the normal and the unstable operating regime of the compressor, including reversed flow conditions. Elements adjacent to the compressor such as inlet pipes, exit volumes and throttles are modeled as required to include their impact on the systems dynamic behavior. The unsteady flow field within the system is determined by solving the unsteady conservation laws for compressible, inviscid flow. Blade forces are determined from the change of aerodynamic momentum across a blade row.

The resulting forces in axial and circumferential direction are used as an input for a direct transient Finite-Element stress analysis. The resulting forces are applied to the blades. The results of the Finite-Element analysis are compared with experimental results from a compressor test rig. Stress is measured by strain-gauges in various positions on the blades. In addition, transient pressure is recorded. Measurements are

taken during normal operation of the compressor as well as during surge. It is shown that the procedure is able to predict the vibration stress level of the blades satisfactorily.

NOMENCLATURE

A	Jacobian matrix
a	speed of sound
E	flux vector
e_t	total energy
H	flux vector matrix
h_t	total enthalpy
I	unity matrix
LE	leading edge
n	rotational speed [rpm]
O	surface vector
P	pressure
R	gas constant
R	source term
t	time
T	temperature
TE	trailing edge
U	state vector
$V_{m,r,\phi}$	meridional, radial, circumferential velocity
V	volume
γ	deviation
κ	ration of specific heat
Λ	eigenvalue matrix
ρ	density
τ	time constant
Ω	rotor shaft speed
ω	loss

INTRODUCTION

On the one hand, many investigations have been performed on the pure aerodynamic aspects of surge. One of the first comprehensive references on this topic are two publications from Greitzer [1,2], where in the first part a non-linear model for the transient performance of a compressor was developed. The occurrence of surge or rotating-stall can be determined with a single parameter. The second paper compares the calculated results with experimental data. It is beyond the scope of this paper to list further publications on the aerodynamic aspects.

On the other hand, few investigations have been performed on the combined aerodynamic and mechanical effects of surge. One of the most detailed papers is that of Mazzawy [3], where the impact of the surge on blades and rotors is described. Birch et al. [4] describe a model for predicting the large impulsive loads that occur during surge in an axial flow compressor. Pressure from a 2-D Navier-Stokes calculation were taken as an input to an Finite-Element Code. Results were compared with a shock-tube experiment.

References [5-7] describe experimental investigations of blade vibration during surge in a centrifugal compressor with various configurations (with/without vaned diffuser; with/without backsweep impeller). Dynamic pressure measurements at the casing along the flow path and strain-gauge measurements were performed.

Fleeter [8] performed a series of experiments in a three stage axial flow research compressor to investigate fundamental aerodynamics of compressor flow instabilities, including rotating stall, surge and unstable modified surge flow regimes between these two modes.

The aerodynamic and structural aspects of surge of a single blade was investigated by Rudy [9]. A Finite-Element code was used for the prediction of the dynamic response. Different load distributions and damping cases were studied. No comparison of numerical results with experimental data was presented.

Quite a lot of publications exist for flutter and forced response analysis, also with coupled fluid/structure approaches. General overviews over these topics are presented by Marshall [10], Slater [11] and Srinivasan [12]. As an example of one of the newest publications in this area the work of Doi is cited [13]. But an application of one of these many procedures to surge or rotating stall is not known to the authors.

Compressors are matched to their environment such that they have sufficient stability margin for conditions, which are possible to occur during operation. However, for extreme conditions in terms of boundary conditions (inlet distortion, ...), engine condition (deterioration, build tolerances, ...) and operating demands (handling, ...), compressor stability cannot be assured for all possible combinations of these factors. Therefore, mechanical blade design has to take into account that compressor instability can occur and that the blades have to withstand the unsteady loads associated with engine instability forms „surge“ and „rotating stall“. A common approach to account for the loads associated with either surge or rotating stall is to use empirical correlations based on experimental data. However, this type of approach is strictly valid only as long as the compressor design is within the parameter space implicitly defined by the experimental set-up from which the correlations have been derived. Any deviation from this parameter space

requires thorough engineering judgement whether these correlations still can be applied.

In contrary, a numerical method which allows calculating the aerodynamic loads associated with surge and/or rotating stall offers the advantage of being independent from any experimentally derived correlations, because it relies only on the laws of physics which describe the behaviour of a fluid.

Both terms “surge” and “rotating stall” describe a highly unsteady state of flow, where flow field properties undergo rapid changes within very short periods of time. Therefore, a fundamental requirement for instability loads prediction is to be able to calculate the flow field accurately in time. Furthermore, both types of compressor instability are strongly influenced not only by local blade properties, but also by the environment within which the compressor is installed, thereby requiring simulating the environment and its interaction with the compressor as well.

The present paper combines the results of an unsteady aerodynamic analysis of surge events with an FEM analysis. Figure 1 shows the general procedure followed in this investigation. Details of the aerodynamic code and the FEM analysis are presented later.

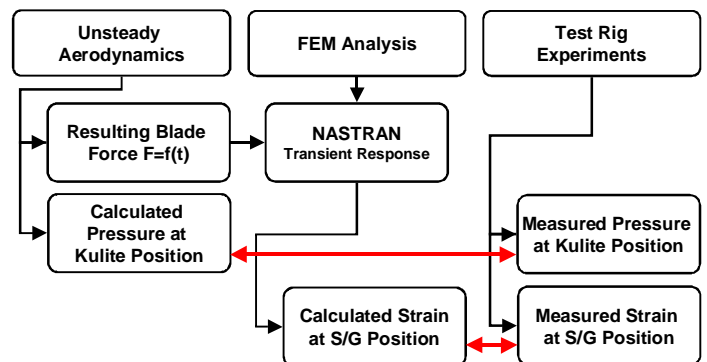


Figure 1: General procedure

AERODYNAMIC CALCULATIONS

Numerical methods, which are widely used for aerodynamic design of blades and are commonly known as Navier-Stokes solvers are not appropriate to serve the task of predicting surge/rotating stall loads. Although they give the best available representation of the flow around a blade, they are much too complex and computationally heavy to be used within the frame of surge/rotating stall load prediction. This prevents the use of complex Navier-Stokes solvers, because a time-accurate calculation of the flow for systems, which consist not only of compressor blades but also of its surrounding environment cannot be achieved within a reasonable time frame. Therefore, simplifications have to be introduced, in order to achieve a reasonable balance between a detailed representation of the flow around the blades and the capability to handle potentially complex system configurations with acceptable amount of time. Typical representations of such models are described by Longley [14] and Demargne et al [15].

The most prominent simplification which has been introduced for the method described in this paper is to represent the flow around the blades by using blade row characteristics to

describe flow losses and turning behaviour. This removes the requirement to perform a detailed calculation of the flow within blade passages, the savings in time due to this simplification are rather used to allow for modelling of all components adjacent to the compressor which influence the flow field both in its initial stages as well as during the fully developed state of compressor instability.

The following passages shortly describe the flow field model, its numerical representation as well as the modelling of fundamental elements of which compression systems are constituted.

NUMERICAL APPROACH

Conservation laws of flow

The numerical method is based on the conservation laws of mass, momentum and energy for an unsteady, compressible flow. The conservation laws are formulated in finite-volume representation for cylindrical coordinate system, representing the meridional and circumferential direction. Currently, the method is not capable of resolving the flow in radial direction as well, therefore, all calculations are performed for an average stream tube.

$$\int \frac{\partial \vec{U}}{\partial t} dV + \oint \vec{H} d\vec{O} = \vec{R}_{Vol} + \vec{R}_{Element} \quad (1)$$

Vector $\vec{R}_{Element}$ represents the influence of arbitrary elements used to build a compression system. For instance, in case of a blade row, pressure losses and turning behaviour are represented by appropriate source terms for the conservation laws of momentum. Further details for blade row modelling are given in the chapter "Blade row modelling". Other types of elements, such as ducts with bleed ports, unbladed ducts with loss generation, etc. are modelled in the same way by introducing their specific behaviour into the corresponding source terms.

The remaining elements of the conservation laws are as follows:

$$\vec{U} = \begin{pmatrix} \rho \\ \rho V_m \\ \rho V_\phi \\ \rho e_t \end{pmatrix} = \text{state vector} \quad (2)$$

$$\vec{H} = \begin{pmatrix} \rho V_m & \rho V_\phi \\ \rho V_m^2 + p & \rho V_\phi V_m \\ \rho V_\phi V_m & \rho V_\phi^2 + p \\ \rho V_m h_t & \rho V_\phi h_t \end{pmatrix} = \text{matrix of flux vectors} \quad (3)$$

$$\vec{O} = \begin{pmatrix} O_m \\ O_\phi \end{pmatrix} = \text{surface vector} \quad (4)$$

$$\vec{R}_{Vol} = \begin{pmatrix} 0 \\ 0 \\ -\int_V \frac{\rho V_r V_\phi}{r} dV \\ 0 \end{pmatrix} \quad (5)$$

= source terms due to representation in cylindrical coordinates

In order to close the system of equations, the state equation for a perfect gas is employed.

$$\frac{p}{\rho} = R \cdot T = \text{state equation for a perfect gas} \quad (6)$$

Functional relationships for inner energy and total enthalpy are as follows:

$$e_t = \frac{1}{\chi - 1} \frac{p}{\rho} + \frac{V_m^2 + V_\phi^2}{2} = \text{inner total energy} \quad (7)$$

$$h_t = \frac{\chi}{\chi - 1} \frac{p}{\rho} + \frac{V_m^2 + V_\phi^2}{2} = e_t + \frac{p}{\rho} = \text{total enthalpy} \quad (8)$$

These equations are used to represent the unsteady, compressible flow field in a two-dimensional cylindrical coordinate system.

Time discretisation

The calculation of unsteady flow requires a time-accurate numerical representation of the flow field, therefore, local time stepping to reduce computation time is not allowed. The advantage of using an implicit time integration in order to decouple the integration time step from limitations resulting from numerical stability requirements has been discarded, because a high resolution in time (resulting in small time steps) was one of the requirements for the procedure, and the additional computational overhead for an implicit procedure had to be balanced against the small benefit of not being able to make full use of possibly larger time steps. Therefore, an explicit time stepping procedure has been employed. The largest possible time step size is dictated from numerical stability requirements which are calculated from local flow conditions as well as the cell size of individual elements, it is defined as follows:

$$\Delta t_{\max} = \min \left(k * \frac{Vol_{i,j} / (O_m + O_\phi)_{i,j}}{|V_{i,j}| + a_{i,j}} \right); \quad k = 0.9-1 \quad (9)$$

Spatial discretisation

The spatial discretisation of the flux balance across a control volume follows a procedure developed by Vinckier [16]. In his approach, the spatial flux balance is split into an upstream and downstream component. This assures numerical stability without being forced to introduce artificial damping terms. The approach is outlined for the one-dimensional conservation laws, and can be transferred to higher dimensions as required.

One-dimensional conservation laws of fluids:

$$\int \frac{\partial \vec{U}}{\partial t} dV + \oint \vec{E} dO = \overline{RS} \quad (10)$$

The flux vector E is represented as follows (making use of its homogeneous property):

$$\vec{E} = \frac{\partial \vec{E}}{\partial \vec{U}} \cdot \vec{U} = \overline{A} \cdot \vec{U} \quad (11)$$

\overline{A} = Jacobi - matrix of E(U)

Using the eigenvalues of A, it follows:

$$\overline{A} = \overline{X} \cdot \overline{\Lambda} \cdot \overline{X}^{-1} \quad (12)$$

$$\overline{A}^{\pm} = \overline{X} \cdot \overline{\Lambda}^{\pm} \cdot \overline{X}^{-1} \quad (13)$$

$$\overline{A} = \overline{A}^{+} + \overline{A}^{-} \quad (14)$$

$\overline{X}, \overline{X}^{-1}$: eigenvector matrix and its inverse

$\overline{\Lambda}, \overline{\Lambda}^{\pm}$: eigenvalues matrix, eigenvalue matrix with only positive resp. only negative eigenvalues

Using these relationships, flux vector E can be transformed as follows:

$$\vec{E} = (\overline{A}^{+} + \overline{A}^{-}) \cdot \vec{U} = (\overline{A}^{+} + \overline{A}^{-}) \cdot \overline{A}^{-1} \cdot \vec{E} \quad (15)$$

$$= \overline{A}^{+} \cdot \overline{A}^{-1} \cdot \vec{E} + \overline{A}^{-} \cdot \overline{A}^{-1} \cdot \vec{E}$$

$$\overline{A}^{\pm} \cdot \overline{A}^{-1} = \overline{X} \cdot \overline{I}^{\pm} \cdot \overline{X}^{-1} \quad (16)$$

\overline{I}^{\pm} = unit matrix, "0" on main diagonal

if the corresponding eigenvalue is not positive resp. not negative

$$\vec{E} = \vec{e}^{+} \cdot \vec{E} + \vec{e}^{-} \cdot \vec{E} \quad (17)$$

$$\vec{e}^{\pm} = \overline{X} \cdot \overline{I}^{\pm} \cdot \overline{X}^{-1}; \quad (18)$$

positive resp. negative flux - filter - matrix

Introducing these relationships finally yields:

$$\int \frac{\partial \vec{U}}{\partial t} dV + \oint (\vec{e}^{+} \cdot \vec{E} + \vec{e}^{-} \cdot \vec{E}) dO = \overline{RS} \quad (19)$$

For the numerical discretisation flux vector E is decomposed into both upstream and downstream weighted components, thereby replacing the spatial integral as follows:

$$\int \frac{\partial \vec{U}}{\partial t} dV + \vec{e}^{+} \cdot (\vec{E}_i \cdot \mathbf{O}_{x,i} - \vec{E}_{i-1} \cdot \mathbf{O}_{x,i-1}) + \vec{e}^{-} \cdot (\vec{E}_{i+1} \cdot \mathbf{O}_{x,i+1} - \vec{E}_i \cdot \mathbf{O}_{x,i}) = \overline{RS} \quad (20)$$

The corresponding equation for the two-dimensional flow field is:

$$\int \frac{\partial \vec{U}}{\partial t} dV + \oint (\vec{e}^{+} \cdot \vec{E} + \vec{e}^{-} \cdot \vec{E}) dO_m + \oint (\vec{f}^{+} \cdot \vec{F} + \vec{f}^{-} \cdot \vec{F}) dO_{\varphi} = \overline{RS} \quad (21)$$

This approach yields the decomposition of flux vectors into upstream and downstream components. The advantage of using flux-filter-matrices is that a spatial weighting of flux differences is achieved which results in a numerically stable discretisation without being forced to introduce artificial damping terms.

Boundary conditions

Boundary conditions at inlet and exit of the computational domain are derived from the theory of characteristics, which demand that a physically meaningful treatment of the flow at inlet resp. exit of the domain requires a split of the flow into waves which propagate in upstream and downstream direction. This split is already achieved with the spatial discretisation approach as described before, the difference now being, that waves entering the computational domain from "infinity" cannot be derived from properties in the interior of the computational domain. Therefore, that part of the spatial discretisation scheme can be used which represents flux propagation from the interior of the domain to the domain boundaries. The missing part, representing incoming waves across both inlet and exit domain boundaries, has to be derived from conditions at "infinity". Typically, total pressure and total temperature are used at the inlet, whereas static pressure forms the boundary condition at the exit of the domain. Details of the implementation can be found in [17].

Within the scope of the procedure described here, it has to be considered, that during engine surge, the flow direction is usually reverted during part of the surge cycle. Therefore, geometric inlet and exit boundaries may not necessarily coincide with physical inlet and exit boundaries. Rather, flow may leave the domain via the inlet and may enter the domain from the back end of the modelled system.

Blade row modelling

As outlined before, the selected approach does not model the detailed flow field within blade row passages, but rather replaces the blade row behaviour by using corresponding characteristics for flow turning and losses.

Usually, blade row characteristics are available for the stable operating regime of a blade row, representing steady-state flow conditions. Therefore, both modelling of operation

beyond the stability limit as well as transient adaptation to new conditions require additional modelling efforts.

Steady-state blade row characteristic

In order to cope with conditions during compressor instability, including periods where flow reversal may occur, blade row characteristics need to be provided which cover the whole of possible blade row operating conditions.

Usually, blade row characteristics cover that part of the operating regime which is associated with stable compressor operation. They are not capable to represent blade row behaviour over the range which is required for prediction of compressor instability, therefore, a procedure is needed to extend available blade row characteristics into the regime of unstable compressor operation.

In order to achieve the required extension of blade row characteristics, the behaviour of compressor stages has been analysed first. The advantage of starting with stage characteristics is that established procedures exist to extend them beyond the stability limit. Sugiyama [18] presents a method to extend stage characteristics into the regime of unstable and reverse flow of a compressor. As sketched in figure 2, stage characteristics are usually provided up to the stability limit, denoted with letter "A". Extension to points "B", "C", "D" is achieved using first-order resp. second-order polynoms, where levels of pressure ratio and efficiency at these points are derived from data at point "A".

As soon as stage characteristics are available for the full operating regime of the compressor during compressor instability, extension of the blade row characteristics can be performed. To this end, stage losses are split between rotor and stator of the stage at a given flow, using a simple loading parameter to achieve a reasonable balance of losses between rotor and stator. Flow turning across the rotor is deduced from energy input across the stage which is only facilitated by the rotor, stator turning follows a simple rule to deduce exit flow angle deviation from inlet incidence.

Unsteady blade row behaviour

The modelling of loss and turning behaviour of blade rows for steady-state operation is described in the preceding paragraph. However, any transient change of operating conditions require to simulate the corresponding transition of blade rows to the new state as well.

In reality, blade rows do not adapt instantaneously to new inlet conditions, but rather need some time for the adaptation. The time needed for adaptation is proportional to the time the flow needs to travel through the blade row. Usually, time lags during transition from one state to another is described by a first-order lag function. Its general form is

$$f(t) + \tau \frac{df}{dt} = f_{ss} \quad (22)$$

$f(t)$ = time-dependent function
 f_{ss} = steady-state final condition

This time lag is to be applied to both blade row losses ω and turning, leading to the following equations for the time-dependent loss and deviation γ of a stator.

$$\omega(t) + \tau_{\omega} \frac{d\omega}{dt} = \omega_{ss} \quad (23)$$

$$\gamma(t) + \tau_{\gamma} \frac{d\gamma}{dt} = \gamma_{ss} \quad (24)$$

In case of a rotor, loss and deviation characteristics are to be applied in the relative frame of reference. In this case, the absolute time derivative has to be split into partial derivatives of time and space to perform the translation into the rotating frame of reference, yielding the following equations.

$$\omega(t) + \tau_{\omega} \left(\frac{\partial \omega}{\partial t} + \Omega \frac{\partial \omega}{\partial \varphi} \right) = \omega_{ss} \quad (25)$$

$$\gamma(t) + \tau_{\gamma} \left(\frac{\partial \gamma}{\partial t} + \Omega \frac{\partial \gamma}{\partial \varphi} \right) = \gamma_{ss} \quad (26)$$

Steady-state values of both losses and deviation are obtained from the blade row characteristics, and are used to derive their time-dependent values.

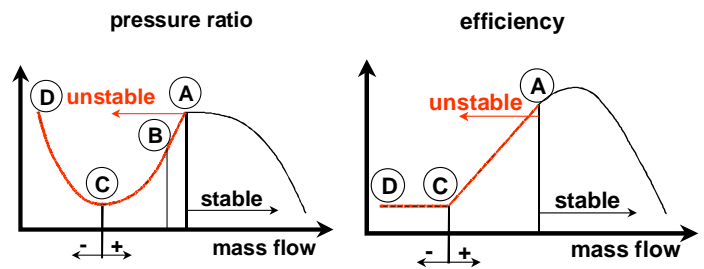


Figure 2: Extension of stage characteristics

Obviously, this approach depends on the availability of suitable time constants. Usually, time constants are provided in non-dimensional form, relative to the transport time of an imaginary particle through the cascade. Typical values of time constants are provided in [18], [19]. These publications also indicate that it is necessary to discern between attached and fully separated flow conditions. Within the scope of the addressed method, this distinction is performed on the basis of flow conditions obtained from the stage characteristics at selected points (Fig. 2). Attached flow is assumed to occur up to point "A" of the stage characteristics, whereas flow between points "B" and "D" is assumed to be fully separated. Between points "A" and "B", the time constant varies linearly.

Representation of blade rows

The interaction between blade rows and flow is mathematically represented by provision of corresponding source terms in the conservation equations of momentum and energy. These source terms are derived from a momentum resp. energy balance across the blade row, assuming known inlet conditions and loss resp. turning characteristics. This yields the exit condition of the blade row (for steady-state flow), from

which the momentum resp. energy difference between inlet and exit can be derived.

Validation of the model

In order to validate the model, extensive comparisons have been performed between measured and calculated data, basically pressures. In the following, some of the results are presented for a 3-stage transonic compressor. The compressor has been equipped with 8 fast-response pressure transducers in front of each rotor. Fig. 3 presents measured traces of static pressure for a surge cycle. For each stage, traces are ordered vertically in accordance with their circumferential position. Data show that compressor surge develops out of a rotating perturbation.

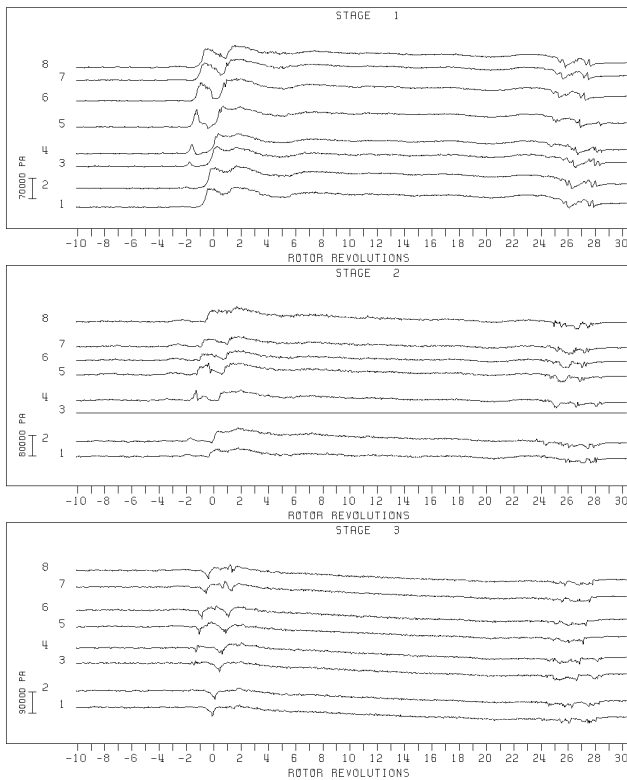


Figure 3: Measured data for a 3-stage transonic compressor

Fig. 4 shows corresponding traces obtained from a calculation. In agreement with measurement data, calculated data also show that compressor surge is preceded by a rotating disturbance with a speed of approx. 50% of rotor shaft speed. The calculation captures both the development history and the rotational speed of the initial disturbance with high accuracy.

Fig. 5 presents a comparison of measured and predicted surge overpressures in front of each stage for the same compressor. Again, the agreement between measurement and numerical simulation is good, not only for the surge overpressure, but also for the time history of pressure between surge initiation and recovery.

Especially the good agreement with respect to surge overpressure is of importance, because this parameter is

occasionally used in empirical correlations as well to deduce surge loads.

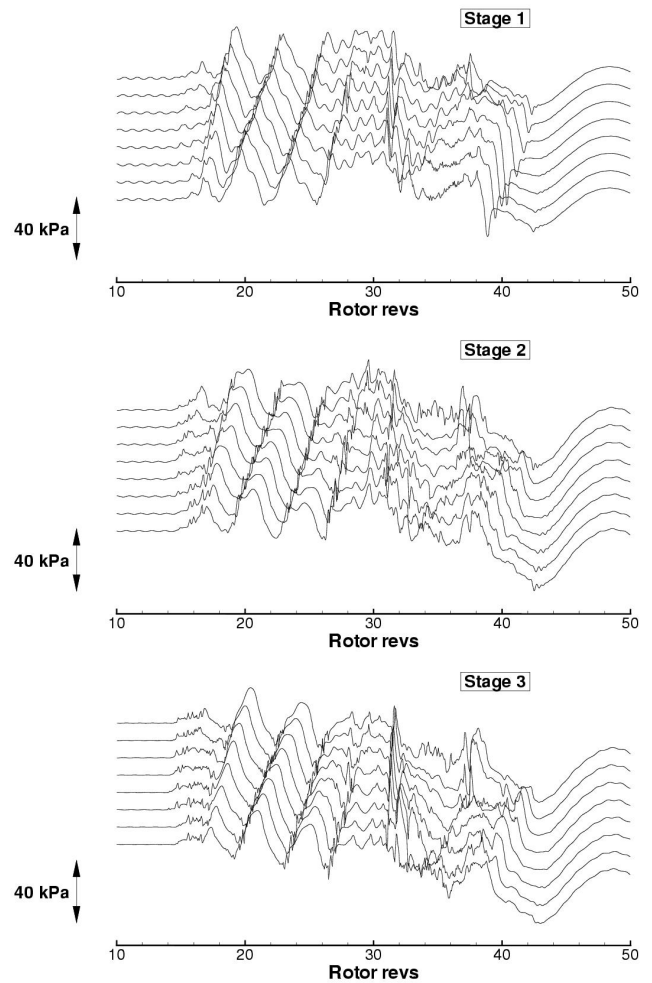


Figure 4: Calculated data for a 3-stage transonic compressor

Time consumption

Because of the selected approach to represent the blade row passage flow field by its loss and turning characteristics, the computational demands of the model are moderate. Calculations for the presented 3-stage compression system (including its modelled environment to capture all influential factors which are of relevance for compressor stability) took only a few hours on a conventional single-processor workstation.

Determination of unsteady blade loads

Although the model has not been intentionally developed to assist in the mechanical design of blades, it turned out that it is quite helpful in predicting surge loads. Forces on the blades in meridional and circumferential direction are simply derived from the difference between inlet and exit momentum for each instant in time, thereby providing the input to FEM models. The model can be run with a time step size compatible with requirements for unsteady FEM calculations (requiring time step sizes in the order of a millisecond or even less).

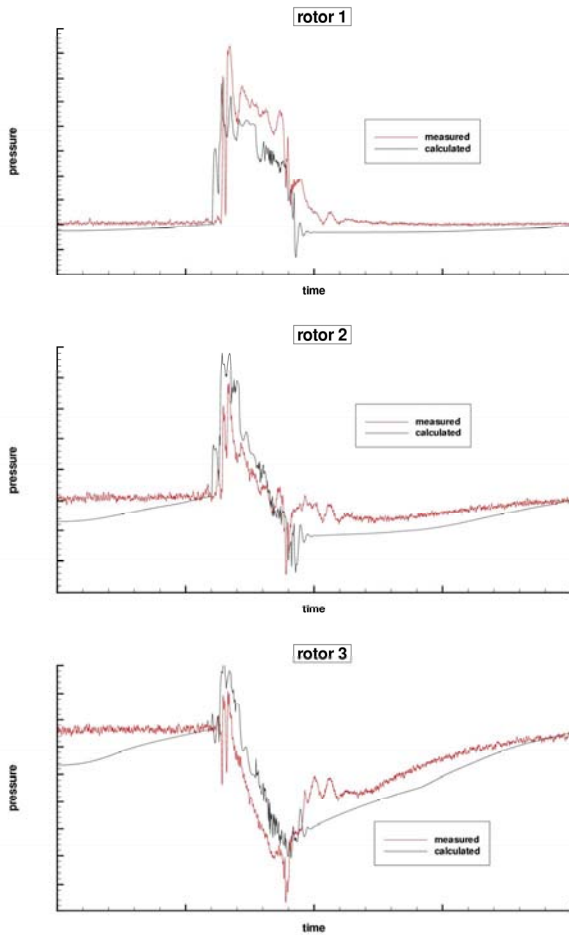


Figure 5: Comparison of measured and predicted surge overpressure (3-stage transonic compressor)

FEM STRUCTURAL ANALYSIS

For the calculation of the structural response to the resulting aerodynamic forces the commercial FEM-code MSC/NASTRAN was used. The transient response option with the resulting force onto the blade as an input was used. The centrifugal forces were applied first as a subcase calculation before the direct transient response calculations were performed. Thus, the deformation of the structure under centrifugal load was taken into account.

The application of the forces onto the blades is a difficult question. For the period of the reversed flow severe separation occurs and even a simulation with unsteady Navier-Stokes codes does not lead to any realistic point of application for the resulting forces. Neither are measurements known to the authors. Thus, engineering judgement has to be used for practical applications.

Here, two different approaches for the application of the unsteady aerodynamic forces are proposed. The first one (Method 1) assumes that the disturbance moves with the speed of sound through the engine and thus also from the trailing edge to the leading edge of the blade (Fig. 6). As the resulting span position of the steady-state forces is at about 60% span, the unsteady force is applied at all nodes along the pressure side at 60% span. This results in a time delay for each single node of $\Delta t = \Delta x / a$ against the trailing edge node, where

$$a = \sqrt{\kappa RT} \quad (27)$$

is the speed of sound calculated with the average blade temperature T . The time delay between trailing edge and leading edge can be seen in the difference between the black and green curve (or red and blue curve) in Fig. 6. The forces are normalized with the steady-state forces so that at zero time the force is unity. The time scale is normalized with the rotor speed ($t^*f = t^*n/60$ [s*rpm/60]).

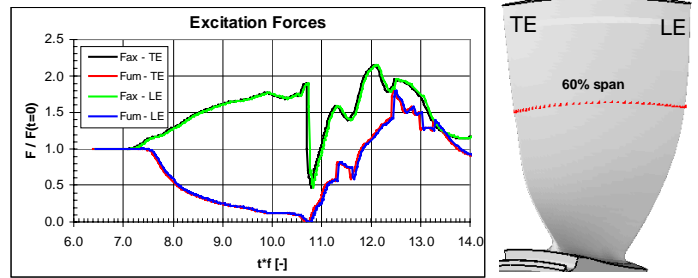


Figure 6: Method 1 for force application

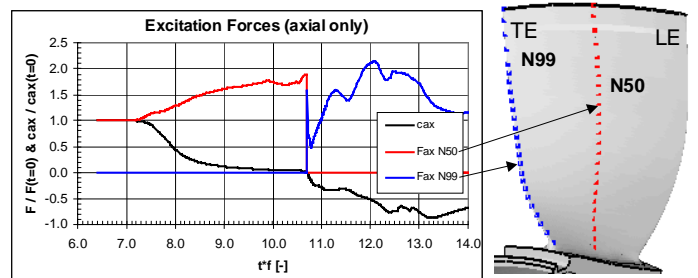


Figure 7: Method 2 for force application

The second approach (Method 2, Fig. 7) assumes that during the normal flow the force is acting at about 50% of the chord length (red curve) and during reversed flow the point of application is on the trailing edge (blue curve). The black curve in the graph indicates the axial velocity which becomes negative at a certain point. From simple velocity triangles during reversed flow it is found that the flow comes nearly perpendicular onto the blade surface at the trailing edge and that this might be a realistic assumption. In order to avoid a single point of contact the force is distributed radial with the same distribution as the normal gas bending force.

EXPERIMENTAL INVESTIGATIONS

The LPC rotor and the first stage disk used in the test rig is presented in Fig. 8 and 9. Figure 10 shows the instrumentation of the first rotor blade of the compressor test rig. Three rotor blades of rotor 1 are equipped with two strain gauges each. One is located close to the leading edge on the pressure side and the other is positioned at the middle of the suction side. Two pressure transducers are located at the casing in front of the rotor blade at two different circumferential positions and one pressure transducer is located at the casing downstream of the rotor blade for the recording of dynamic pressure.



Figure 8: LPC rotor



Figure 9: 1st stage blisk

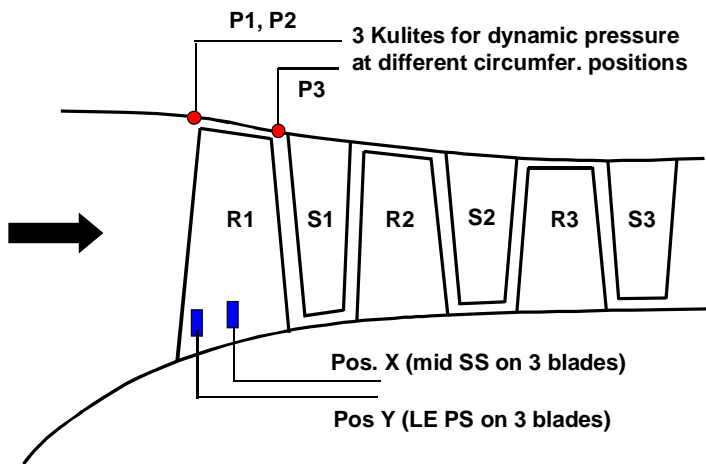


Figure 10: Rig instrumentation

The results of the measurements are presented in the next section along with the calculations.

DISCUSSION OF RESULTS

Figure 11 shows the aerodynamic model of the compressor rig. In Figure 12 the casing pressure in front of the first rotor and the axial velocity in the first rotor as they are predicted from the aerodynamic code are presented. Both values are normalized with the steady-state values. The pressure overshoot is 106%. The magnitude of the velocity during the reversed flow phase goes up to about 80% compared with the normal flow conditions, but into the opposite direction. The duration of the total surge event is predicted to be about 40.

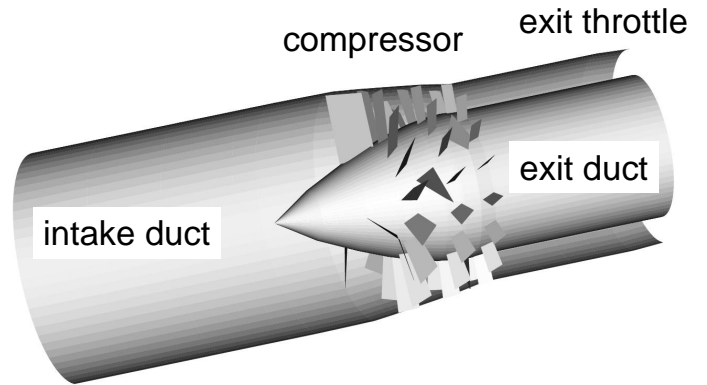


Figure 11: Aerodynamic model compressor rig

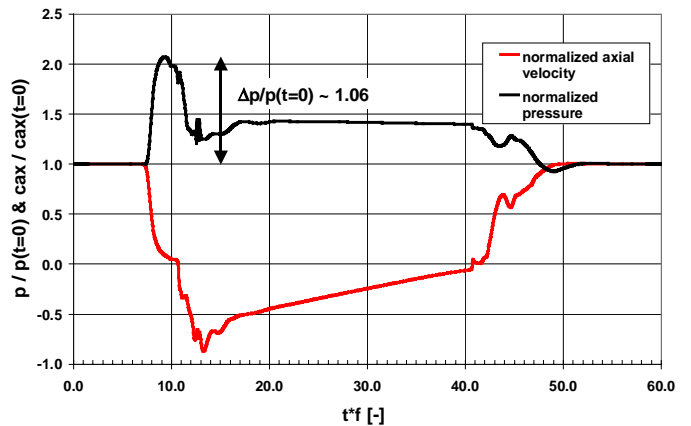


Figure 12: Calculated pressure and axial velocity in front of rotor 1

Figure 13 shows the corresponding experimental pressure. The data are filtered with 50Hz in order to suppress noise. The pressure was normalized with the same value as the calculated graph. The pressure overshoot is 101%, which agrees very well with the calculation. The duration of the event is about 50, which is slightly longer than the predicted duration. The overall agreement between experiment and numerical analysis is quite good.

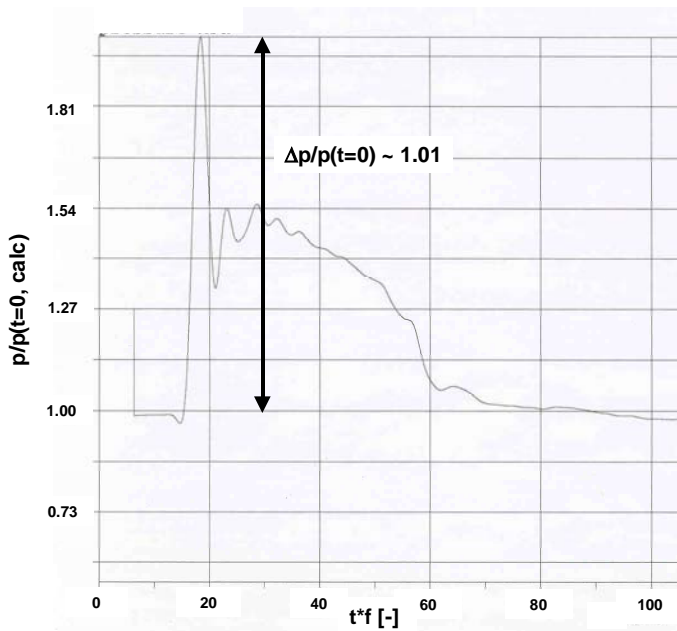


Figure 13: Measured pressure in front of rotor 1

In Figure 14 the axial and circumferential blade forces as they come from the unsteady aerodynamics are displayed. As the highest stress amplitude is to be expected to occur after the very sharp axial force reduction at $t^*f \sim 10.7$, the force input into NASTRAN was kept constant after $t^*f = 15$. Due to the high computational time the FEM calculation was only carried out up to $t^*f = 27$. A quite small time step had to be chosen in order to capture the dynamics of the blade. A time step of less than 1% of the first bending mode cycle period was chosen. The calculation was performed without damping because it was found that the low damping associated with blisks has a negligible influence on the maximum vibration stress, which is of interest to the engineer (see also Ref. [9]).

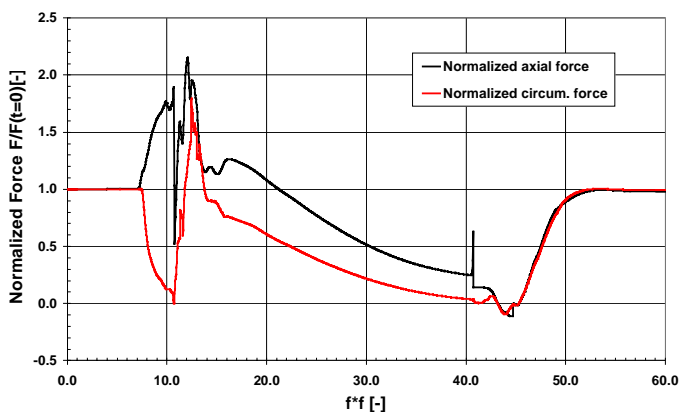


Figure 14: Calculated axial and circumferential unsteady blade force

Figure 15 presents the results of the stress history at the two strain gauge positions X (black line) and Y (red line) for the two methods. The stress was normalized with the average of the three strain-gauge readings at the corresponding position. For the method 1 vibration stress amplitudes (0-peak) of 0.7

and 0.63 can be found for the positions X and Y. Method 2 results in higher amplitudes. Here, the values are 0.86 and 0.93, respectively.

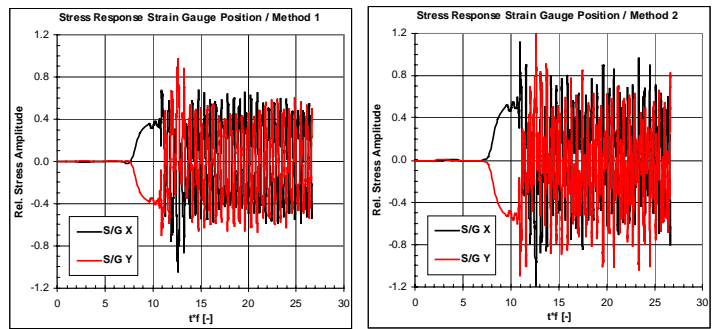


Figure 15: Calculated stress at S/G positions

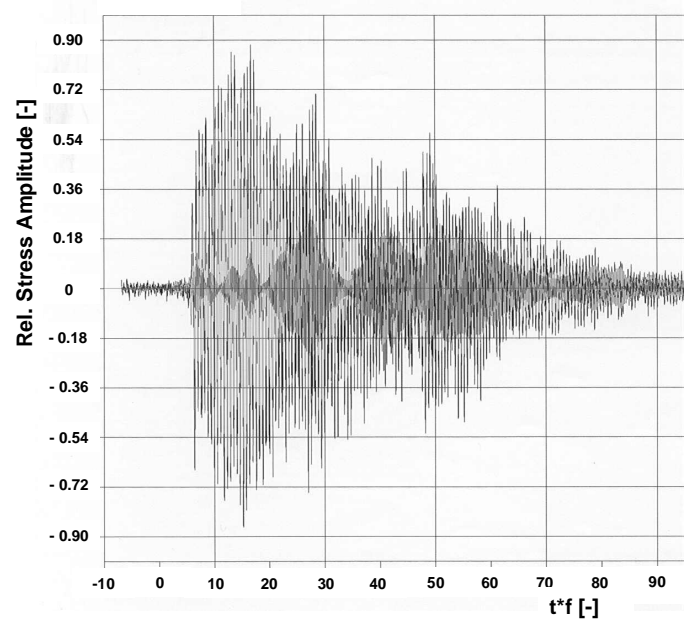


Figure 16: Measured stress at S/G position X

Figure 16 shows the corresponding experimental measurement of the strain gauge at position X. The measured strain was converted to normalized stress so that the y-axis can directly be compared to the calculations. The time axis was shifted so that the beginning of the surge coincides with the numerical simulation. The qualitative agreement between the measured and calculated stress response is quite good, keeping in mind that the calculation was performed without damping.

A quantitative comparison is presented in Figure 17. Here, for both positions X and Y the maximum vibration stress amplitude for all three strain gauge signals and the two calculated values are compared. It can be observed that there is some scatter in the experimental data. While method 1 underestimates the average value of the experimental data by about 30%, method 2 comes much closer to the mean values. However, the authors had other test cases where the tendency was vice-versa. Thus, more test cases have to be analyzed before a clear indication for one of the two methods is obtained.

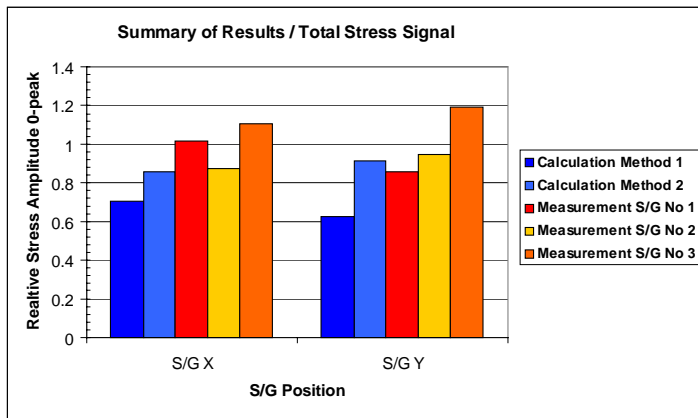


Figure 17: Comparison of Measurement and Calculation

The calculation procedure presented here is very helpful in understanding the dynamic response of blades during surge. The quantitative comparison with experimental results is satisfactorily, but some effort remains to be done to get even better agreements.

CONCLUSIONS

A numerical procedure was presented which allows time-accurate modeling of a compression system during compressor instability. The procedure has been used to calculate unsteady blade forces during surge, and its output has been used as input to an unsteady FEM calculation. The comparison between calculated and measured transient pressures shows good agreement.

The application of the unsteady blade forces onto the blades during surge was done with two different approaches. Both methods give quite good agreements with experimental data from strain-gauge measurements in a compressor test rig, underestimating the vibration stress response by some amount. Nevertheless, the calculation procedure presented here is very helpful in understanding the dynamic response of blades during surge not only in the design phase.

Future work will be aimed at a more realistic distribution of the forces on the whole blade surface. More comparisons with experimental strain-gauge data during surge are necessary in order to show which of the two methods for the force application yields the better results for a higher number of test cases. The two-dimensional fluid flow code will be extended to three dimensions.

REFERENCES

[1] Greitzer, E. M., 1975, "Surge and rotating stall in axial flow compressors – Part 1: Theoretical compression system model", ASME-paper 75-GT-9
 [2] Greitzer, E. M., 1975, "Surge and rotating stall in axial flow compressors – Part 2: Experimental results and comparison with theory", ASME-paper 75-GT-10

[3] Mazzawy, R. S., 1979, "Surge-Induced Structural Loads in Gas Turbines", ASME-paper 79-GT-91
 [4] Birch, N. T., Brownell, J. B., Cargill, A. M., Lawson, M. R., Parker, R. J., Tillen, K. G., 1988 "Structural loads due to surge in an axial compressor", ImechE, pp. 117-124
 [5] Haupt, U., Rautenberg, M., 1985, "Investigation of blade vibration during surge of a centrifugal compressor", ISABE-paper 85-7085
 [6] Jin, D., Haupt, U., Seidel, U., Rautenberg, M., 1987, "On the mechanism of blade excitation due to surge on centrifugal compressors", Proc. Intern. Gas Turbine Congress. Tokyo 1987, III, pp. 341-348
 [7] Jin, D., Haupt, U., Hasemann, H., Rautenberg, M., 1992, "Excitation of blade vibration due to surge of centrifugal compressors", ASME-paper 92-GT-149
 [8] Kim, K. H., Fleeter, S., 1992, "Compressor unsteady aerodynamic response to rotating stall and surge excitations", AIAA-paper 93-2087
 [9] Rudy, M. D., 1982, "Transient blade response due to surge induced structural loads", SAE Technical paper 821438
 [10] Marshall, J. G., Imregun, M., 1996, "A Review of Aeroelasticity Methods with Emphasis on Turbomachinery Applications", Journal of Fluids and Structures, 10, pp. 237-267
 [11] Slater, J. C.; Minkiewicz, G. R.; Blair, A. J., 1998, "Forced response of bladed disk assemblies - a survey", AIAA-paper 98-3743
 [12] Srinivasan, A. V., 1997, "Flutter and resonant vibration characteristics of engine blades", The 1997 IGTI scholar paper, Journal of Engineering for Gas Turbines and Power, 119, pp. 742-775
 [13] Doi, H.; Alonso, J. J., 2002, "Fluid/structure coupled aeroelastic computations for transonic flows in turbomachinery", ASME-paper GT-2002-30313
 [14] Longley, J. P., 1997, "Calculating the Flowfield Behavior of High-Speed Multi-Stage Compressors", ASME paper 97-GT-467
 [15] Demargne, A. A., Longley, J. P., 1997, "Comparisons Between Measured and Calculated Stall Development in Four High-Speed Multi-Stage Compressors", ASME paper 97-GT-468
 [16] Vinckier, A., 1991 "An Upwind Scheme Using Flux Filters Applied to the Quasi 1D-Euler Equations", Zeitschrift für Flugwissenschaft und Weltraumforschung, 15, pp. 311 – 318
 [17] Veuillot, J.P., Meauze, G., 1985, "A 3D Euler Method for Internal Transonic Flows Computation with a Multi-Domain Approach", AGARD Lecture Series 140
 [18] Sugiyama, Y., 1984, "Surge Transient Simulation in Turbo-Jet Engine", Ph.D. Thesis, University of Cincinnati, Department of Aerospace Engineering and Applied Mechanics
 [19] Nagano, S. Y., Machida, Y., Takata, H., 1971, "Dynamic Performance of Stalled Blade Rows", Tokyo Joint International Gas Turbine Conference and Product Show